Photocatalytic Degradation of Basic Violet 4: Degradation Efficiency, Product Distribution, and Mechanisms

Chiingchang Chen* and Chungshin Lu

Department of General Education, National Taichung Nursing College, Taichung 403 Taiwan, China

Received: May 20, 2007; In Final Form: July 14, 2007

The photocatalytic degradation of Basic Violet 4 (BV-4) was examined in aqueous TiO_2 suspensions under UV light irradiation. After 30 W UV 365 nm irradiation for 20 h, approximately 99.9% of BV-4 was degraded. The techniques of high performance liquid chromatography-photodiode array-electrospray ionization-mass spectrometry (HPLC-PDA-ESI-MS), gas chromatography-mass spectrometry (GC-MS), and total organic carbon (TOC) have been used to identify the various photodecomposed products and to investigate the photocatalytic mechanism of the dye after low watt irradiation. The degradation progresses through competitive reactions such as *N*-de-ethylation and destruction of the conjugated structure. The *N*-de-ethylation took place in a stepwise manner to yield mono-, di-, tri-, tetra-, penta-, and hexa-*N*-de-ethylated BV-4 species while the destruction of the conjugated structure yielded 4-diethylaminophenol (DAP), 4-diethylamino-4′-diethylaminobenzophenone (DDBP), and their *N*-de-ethylated products in the TiO_2-mediated photocatalysis process. Moreover, the hydroxyethylated intermediates formed by the *N*-de-ethylated BV-4, DDBP, and DAP processes were separated and identified. The GC-MS analysis showed the formation of *N*,*N*-diethylaminobenzene, *N*-ethylaminobenzene, aminobenzene, acetamide, 2-propenoic acid, and acetic acid. Nonetheless, we clearly observed the changes in the distribution of each intermediate during the photodegradation of BV-4. For decolorization of dyes, the possible photodegradation pathways were proposed and discussed on the basis of the evidence of intermediates formation.

1. Introduction

Over 700 000 tons of dyes and pigments are produced annually worldwide, of which about 20% are in industrial effluents from the textile dyeing and finishing processes.[1] Many of these synthetic "dyestuffs" cannot be treated successfully by conventional methods because of their complex polyaromatic structure, and hence, they cause health problems.[2] Triphenylmethane dyes are used extensively in the textile industry for dying nylon, cotton, wool, and silk, as well as for coloring oils, fats, waxes, varnishes, and plastics. The paper, food, cosmetic, and leather industries are also major consumers of these dyes. Additionally, they are applied as staining agents in bacteriological and histopathological processes.[3,4] The photocytotoxicity of triphenylmethane dyes based on reactive oxygen species production is tested intensively with regard to their photodynamic therapy.[5,6] Thyroid peroxidase-catalyzed oxidation of the triphenylmethane dyes results in the formation of various *N*-dealkylated primary and secondary aromatic amines, which have structures similar to aromatic amine carcinogens.[7] Previous studies[8,9] on photocatalytic degradation of nitrogen-containing aromatics demonstrated that either photogenerated electrons or hydroxyl radicals act concurrently to transform the nitrogen-containing groups.

TiO_2 is broadly used as a photocatalyst because it is photochemically stable and nontoxic and has a low cost. The TiO_2-mediated photocatalysis process has been successfully used to degrade dye pollutants in the past decades.[10−16] Studies on photocatalytic degradation of different kinds of organics have been reported in the literature, and most of them included a detailed examination of the so-called primary processes under different working conditions.[17,18] However, less attention has been paid to the study of the degradation mechanism and to the identification of major transient intermediates, which have been recognized as very important aspects of these processes recently, especially in view of their practical applications.

In earlier reports,[19−21] it was noted that some of the triphenylmethane dyes that contain *N*-alkylamine groups appeared to photodegrade via two competitive pathways: one was *N*-de-alkylation of the chromophore skeleton, which has been sufficiently studied,[22] and the other was cleavage of the whole conjugated chromophore structure, which has never been studied sufficiently, in the TiO_2-assisted photodegradation system. The mechanistic details remained uncertain.

By using high performance liquid chromatography-photodiode array-electrospray ionization-mass spectrometry (HPLC-PDA-ESI-MS), gas chromatography-mass spectrometry (GC-MS), and total organic carbon (TOC), we identify the purpose of this research is to identify the reaction intermediates and to understand the detail mechanism on the photodegradation of Basic Violet 4 (BV-4) dye when it is under the TiO_2/UV process. We hope the results can be a foundation for future applications.

2. Experimental Section

2.1. Reagents and Materials. The TiO_2 powder (Degussa P25), a mixture of anatase and rutile (8:2), was used as received as a photocatalyst without further purification. BV-4 (ethyl violet; *N*,*N*,*N*′,*N*′,*N*″,*N*″-hexaethylpararosaniline) was obtained from Tokyo Kasei Kogyo Company and used as such without further purification. The chemical structure of BV-4 is shown

* Author to whom correspondence should be addressed. E-mail: ccchen@ntcnc.edu.tw or ccchen@mail.ntcnc.edu.tw. Phone: 886-4-2219-6975. Fax: 886-4-2219-4990.

10.1021/jp0738964 CCC: $37.00
Published on Web 08/22/2007

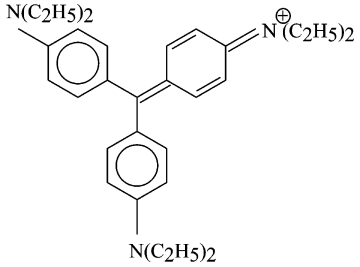

Figure 1. Chemical structure of Basic Violet 4.

in Figure 1. 4-Aminophenol (AP; analytical standard) was purchased from Riedel-de Haen. The 4-(*N*,*N*-diethylamino)-4′-(*N*′,*N*′-diethylamino)benzophenone (DDBP) was obtained from Tokyo Kasei Kogyo Company. Reagent-grade ammonium acetate, nitric acid, and sodium hydroxide and HPLC-grade methanol were purchased from Merck.

2.2. Apparatus and Instruments. The following instruments were used: a GC-MS system, equipped with a AutoSystem XL gas chromatograph and a Perkin-Elmer TurboMass Gold mass spectrometer; a Waters ZQ LC/MS system, equipped with Waters 1525 Binary HPLC pumps, a Waters 2996 photodiode array detector, a Waters 717plus autosampler, and a Waters micromass-ZQ4000 detector; a Tekmar-Dohrmann Phoenix 8000 TOC analyzer, equipped with a nondispersive infrared (NDIR) detector and automatic syringe injection. The C-75 Chromato-Vue Cabinet of UVP provides a wide area of illumination from the 15 W 365 nm tubes positioned on two sides of the cabinet interior.

2.3. Photodegradation Experiments. An aqueous TiO_2 dispersion was prepared by adding 50 mg of TiO_2 powder to a 100 mL solution containing the BV-4 at appropriate concentrations. For reaction in different pH media, the initial pH of the suspensions was adjusted by addition of either a NaOH or a HNO_3 solution. Prior to irradiation, the dispersions were magnetically stirred in the dark for approximately 30 min to ensure the establishment of the adsorption−desorption equilibrium. Irradiations were carried out using two lamps (UV 365 nm, 15 W). At given irradiation time intervals, the dispersion was sampled (5 mL), centrifuged, and subsequently filtered through a Millipore filter (pore size 0.22 μm) to separate the TiO_2 particles.

Blank experiments in the flask without addition of TiO_2 showed a little decolorization of the irradiated solution. It proved the expected instability of BV-4 dye under UV light irradiation. Addition of 0.5 g L^{-1} TiO_2 to solutions containing 50 mg L^{-1} of BV-4 did not alter the stability of the dye in the dark.

2.4. Analytical Methods. The mineralization of the dye was monitored by measuring the TOC content with a Tekmar-Dohrmann Phoenix 8000 TOC analyzer by directly injecting the aqueous solution.

The degradation was monitored by measuring the absorbance with a PDA detector. After each irradiation cycle, the amount of the residual dye was determined by HPLC-PDA. The analysis of organic intermediates was accomplished by HPLC-PDA-ESI-MS after the readjustment of the chromatographic conditions in order to make the mobile phase compatible with the working conditions of the mass spectrometer. Two different kinds of eluent were employed in this study. Solvent A was 25 mM aqueous ammonium acetate buffer (pH 6.9) while solvent B was methanol. LC was carried out on an Atlantis dC18 column (250 mm × 4.6 mm i.d., dp = 5 μm). The flow rate of the mobile phase was set at 1.0 mL min^{-1}. A linear gradient was set as follows: $t = 0$ min, $A = 95$, $B = 5$; $t = 20$ min, $A = 50$, $B = 50$; $t = 40-45$ min, $A = 10$, $B = 90$; $t = 48$ min, $A = 95$, $B = 5$. The column effluent was introduced into the ESI source of the mass spectrometer.

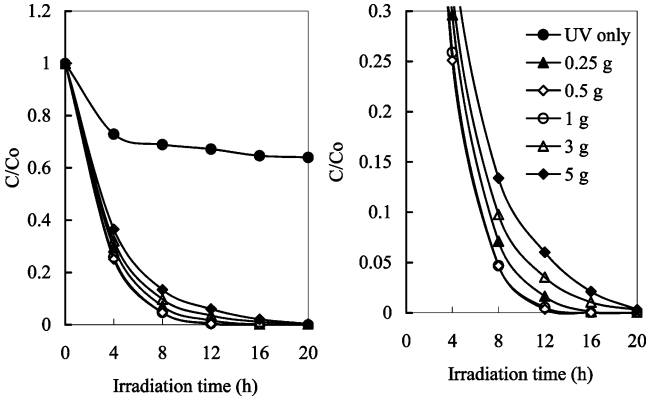

Figure 2. Influence of catalyst concentration was examined by the degradation rate for the decomposition of BV-4. The value of C/Co was expanded on the right. Experimental condition: dye concentration (50 mg L^{-1}), absorbance was followed at 580 nm, continuous stirring, and irradiation time 20 h.

Solid-phase extraction (SPE) was employed for preconcentration of irradiated samples prior to GC-MS analysis. Oasis HLB (hydrophilic/lipophilic balance) was used as the sorbent, and this ensures good recovery of compounds in a wide range of polarities. The cartridges were placed in a vaccum cube (provided by Supelco) and conditioned with 5 mL of methanol and 5 mL of deionized water. After the conditioning step, 1000 mL aliquots of the irradiated samples were loaded at a flow rate of approximately 10 mL/min. Elution was performed with 5 mL of methanol. The eluates obtained were concentrated by solvent evaporation with a gentle nitrogen stream and recomposed to a final volume of 1 mL in methanol. The extracts were stored in amber vials and refrigerated until chromatographic analysis to prevent further degradation.

GC/MS analyses were run on a Perkin-Elmer AutoSystem-XL gas chromatograph interfaced to a TurboMass selective mass detector. Separation was carried out in a DB-5 capillary column (5% diphenyl/95% dimethyl-siloxane), 60 m, 0.25 mm inner diameter, and 1.0 μm thick film. A split-splitless injector was used under the following conditions: injection volume 1 μL, injector temperature 280 °C, split flow 10 mL/min. The helium carrier gas flow was 1 mL/min. The oven temperature program was 4.0 min at 40 °C, 4 °C/min to 80 °C (2 min), 8 °C/min to 280 °C (9 min). The autotuning software optimized typical MSD operating conditions. Electron impact (EI) mass spectra were monitored from 35 to 300 *m*/*z*. The ion source and inlet line temperatures were set at 220 and 280 °C, respectively.

3. Results and Discussion

3.1. Effect of Photocatalyst Concentration. In slurry photocatalytic processes, the amount of photocatalyst is an important parameter that can affect the degradation rate of organic compounds. The optimal catalyst concentrations reported in the literature for TiO_2 Degussa P25 range from 0.1 to 5.0 g L^{-1}, depending on the nature of the compounds and the photoreactor geometry.[23] Hence, the effect of photocatalyst concentration on the photodegradation rates of the BV-4 dye was investigated by employing different concentrations of TiO_2 varying from 0 (UV only) to 5.0 g L^{-1}. As expected, the photodegradation rate of the BV-4 was found to increase then decrease with the increase in the catalyst concentration (Figure 2). This is characteristic of heterogeneous photocatalysts, and the results

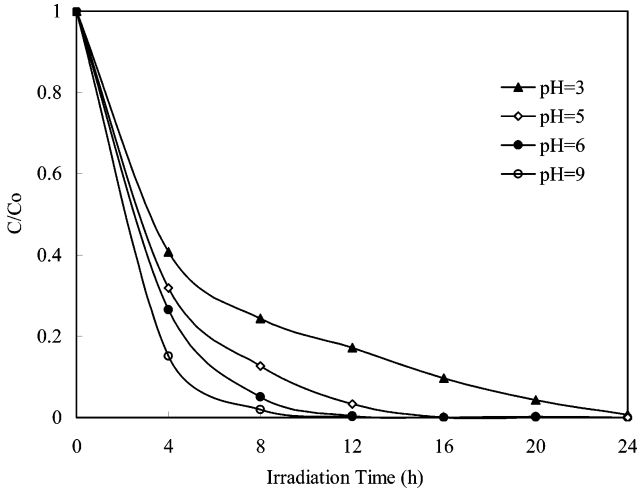

Figure 3. pH effect on the BV-4 degradation rate: TiO_2, 50 mg L^{-1}; BV-4, 500 mg L^{-1}.

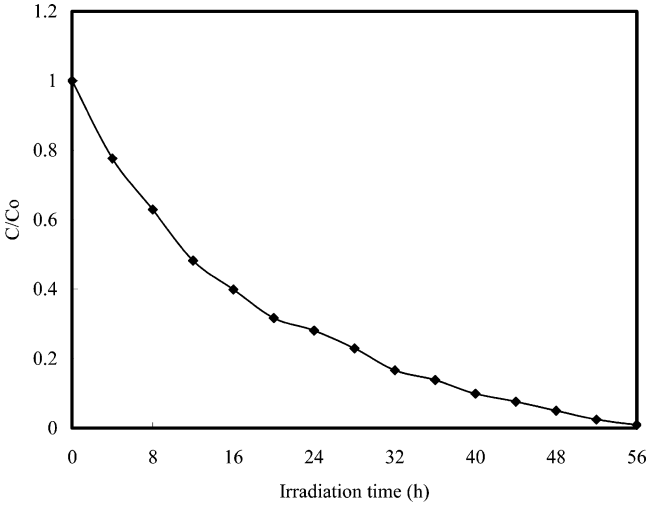

Figure 4. Depletion in TOC as a function of irradiation time for an aqueous solution of BV-4 in the presence of TiO_2. Experimental condition: dye concentration (50 mg L^{-1}), P25 (500 mg L^{-1}), pH 6, absorbance was followed at 580 nm, continuous stirring, and irradiation time 56 h.

are in agreement with the earlier studies.[18] The photolysis reaction resulted in a decrease about 38% in the BV-4 concentration after 20 h while, in the photocatalytic reaction, the BV-4 was completely decomposed after 20 h. Above 0.5 g L^{-1} of TiO_2, the initial rate of BV-4 degradation was not affected further by a progressive increase in TiO_2 concentration. The maximal initial degradation rate for BV-4 appears at a TiO_2 concentration of around 0.5−1.0 g L^{-1}. This phenomenon may be due to the aggregation of TiO_2 particles at high concentrations causing a decrease in the number of surface active sites. It is known, however, that a practical limit of the scattering light (around 1−2 g L^{-1}) exists, above which the degradation rate will decrease because of the reduction of the photonic flux within the irradiated solution.[24] In the following experiment, we chose 0.5 g L^{-1} of TiO_2 as the optimum dosage.

3.2. Observed pH Effect. The surface of TiO_2 would charge negatively and adsorb cationic species easily under pH > pH_{zpc} (zero point charge) conditions. In the reverse condition, it would adsorb anionic ones.[25] However, the adorption of the substrate onto the TiO_2 surface directly affects the occurrence of electron transfer between the excited dye and the TiO_2 and further influences the degradation rate. The surface becomes positively charged, and the number of adsorption sites may decrease above the isoelectric point of TiO_2.

The photodegradation rate of the BV-4 as a function of reaction pH is shown in Figure 3. This rate was found to increase with increases in the value of pH. The chromatograms recorded at 580 nm at different pH values are illustrated in Supporting Information (Figure 7). Under acidic conditions, the cationic BV-4 dye was found difficult to adsorb onto the TiO_2 surface, usually with the active •OH radicals formed in low concentrations, and hence the photodegradation rate of BV-4 remained slow. With higher pH values, the formation of active •OH species is favored. Not only the transfer from holes to the adsorbed hydroxyls have been improved, but also the electrostatic abstractive effects between the negatively charged TiO_2 particles and the operating cationic dyes have been improved. In accord with the data of Figure 3, we presume that the conjugated structure of BV-4 is efficiently destroyed and that the *N*-de-ethylation of BV-4 occurs to a rather small extent under acid conditions while the result is just the opposite under basic conditions. Although the BV-4 dye can be adsorbed onto the TiO_2 surface to some extent in alkaline media, when the pH value is too high, the dye molecules will change into the colorless carbinol base.[16,26] In a good agreement with the adsorption mechanism proposed,[20] our results indicate that the TiO_2 surface is negatively charged and that the BV-4 was adsorbed onto the TiO_2 surface through the positive ammonium groups.

3.3. UV-Visible Spectra. The changes of the UV−vis spectra during the photodegradation process of the BV-4 dye in the aqueous TiO_2 dispersions under UV irradiation are illustrated in Supporting Information (Figure 8). After UV irradiation for 20 h, approximately 99.9% of the BV-4 dyes was degraded. The characteristic absorption band of the dye around 589.6 nm decreased rapidly with slight hypsochromic shifts (575.4 nm), but no new absorption bands appeared even in the UV range (λ > 200 nm), which indicated that a series of *N*-de-ethylated intermediates may have formed and the whole conjugated chromophore structure of the BV-4 dye may have been cleaved.

3.4. Evolution of TOC. The complete mineralization of 1 mol BV-4 dye molecule implies the formation of the equivalent amount (31 mol) of CO_3^{2-} at the end of the treatment. However, the depletion in TOC (shown in Figure 4) clearly indicates that the reaction does not go to completion. In fact, after 56 h irradiation, about 99.9% of the initial organic carbon has been transformed into CO_2, which implied that there still existed other organic compounds in the irradiated solution. This is supported by the HPLC-PDA analysis, which suggests the presence of residual organic products even after 56 h irradiation, confirming the noticeable degradation of the examined dye. These findings are in agreement with those obtained in a study concerning the photocatalytic degradation of anthraquinone, where the persistence of various aromatic compounds was reported even after long-term irradiation.[27]

3.5. Separation of the Intermediates. Temporal variations occurring in the solution of BV-4 dye during the degradation process with UV irradiation were examined using HPLC coupled with a photodiode array detector and ESI mass spectrometry. The chromatograms at different pH values are illustrated in Figure 5a,b and recorded at 580 or 300 nm. With irradiation up to 12 h at pH 6 and 24 h at pH 3, 33 components were identified, all with retention times of less than 50 min. We denoted the BV-4 dye and its related intermediates as species **A**−**I**, **A′**−**F′**, **a**−**f**, **a′**−**d′**, and $\alpha-\gamma$. Except for the initial BV-4 dye (peak A), the other peaks initially increased before subsequently decreasing, indicating formation and transformation of the

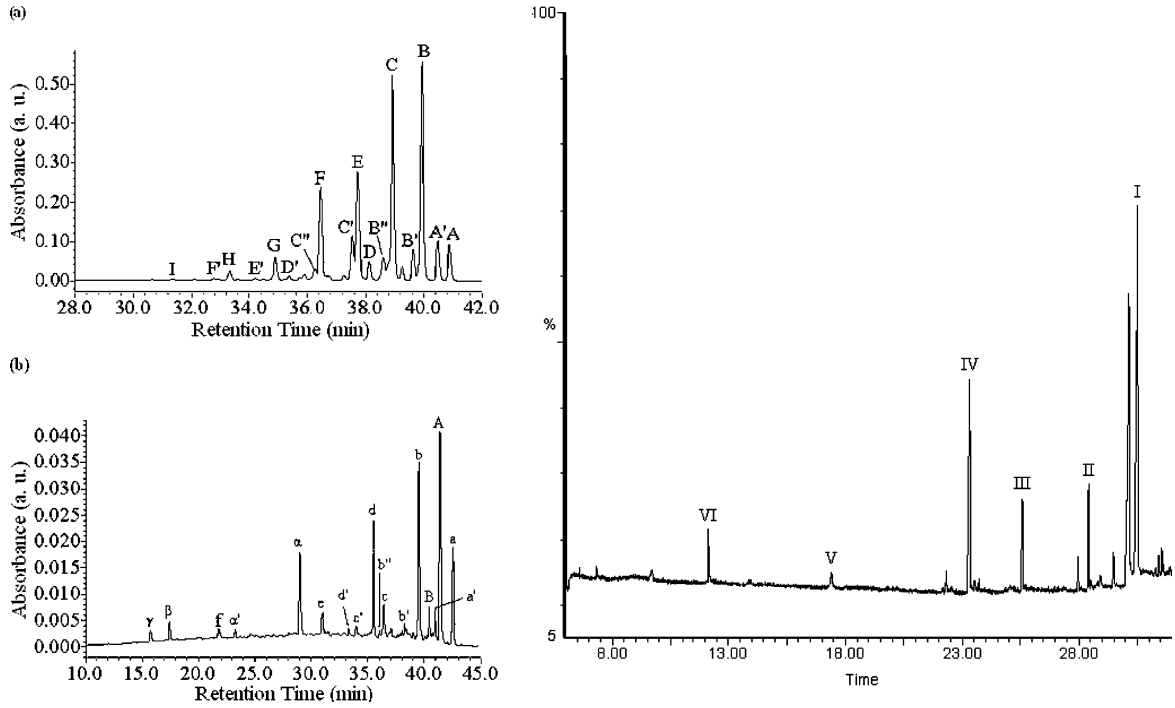

Figure 5. HPLC chromatogram of (a) the *N*-de-ethylated intermediates at pH 6, 12 h, recorded at 580 nm and (b) the destruction of the conjugated structure of the BV-4 at pH 3, 24 h, recorded at 300 nm; (c) GC-MS/EI chromatogram obtained for a SPE extract of solution after 32 h of irradiation with UV light.

intermediates. Figure 5c shows the GC-MS chromatogram obtained for an SPE extract of BV-4 solution after 32 h of irradiation. Up to six compounds could be detected as possible degradation intermediates. We denoted these intermediates as compounds **I**−**VI**.

3.6. Identification of the Intermediates. *3.6.1. UV-Visible Spectra of the Intermediates.* The absorption spectra of each intermediate in the visible and ultraviolet spectral region are depicted in Supporting Information (Figure 9). They are identified as **A**−**I** and **A′**−**F′** corresponding to the peaks A−I and A′−F′ in Figure 5a, respectively. The other intermediates are identified as **a**−**f**, **a′**−**d′**, and α−γ, corresponding to the peaks a−f, a′−d′, and α−γ in Figure 5b. The absorption maximum of the spectral bands shifts from 589.6 nm (spectrum A) to 556.6 nm (spectrum I), 618.9 nm (spectrum A′) to 576.1 nm (spectrum F′), 379.5 nm (spectrum a) to 339.1 nm (spectrum f), 379.5 nm (Figure 5b, peak a′) to 341.5 nm (peak d′), and 305.7 nm (peak α) to 281.9 nm (peak γ). These shifts of the absorption band are presumed to result from the formation of a series of *N*-de-ethylated or *N*-hydroxyethylated intermediates. From these results, several groups of intermediates can be distinguished.

The first and second groups are marked in the chromatogram and illustrated in Figure 5a. The *N*-de-ethylation of the BV-4 dye and the *N*-hydroxyethylated intermediates of the *N*-de-ethylated BV-4 species have the wavelength position of their major absorption band moved toward the blue region, λ_{max}, **A** (BV-4), 589.6 nm; **B**, 584.7 nm; **C**, 577.3 nm; **D**, 578.9 nm; **E**, 576.1 nm; **F**, 578.6 nm; **G**, 567.6 nm; **H**, 573.7 nm; **I**, 556.6 nm; **J**, 550.3 nm; **A′**, 618.9 nm; **B′**, 598.2 nm; **B″**, 601.7 nm; **C′**, 578.6 nm; **C″**, 584.7 nm; **D′**, 585.9 nm; **E′**, 570.9.4 nm; and **F′**, 576.1 nm. The *N*-de-ethylation of the BV-4 dye caused the wavelength shifts depicted in Supporting Information (Figure 9a) because of the attack by one of the active oxygen species on the *N*,*N*-diethyl or *N*-ethyl groups. Examination of Supporting Information suggests that BV-4 dye is *N*-de-ethylated in a stepwise manner by *N*-hydroxyethylated intermediate (i.e., ethyl groups are removed one by one as confirmed by the gradual peak wavelength shifts toward the blue region), which has been reported.[22]

The third and fourth groups are marked in the chromatogram and illustrated in Figure 5b. Destruction of BV-4 yields DAP, DDBP, and their *N*-de-ethylated products *N*-hydroxyethylated intermediate. The *N*-de-ethylation of the DDBP and the *N*-hydroxyethylated intermediates of the *N*-de-ethylated DDBP species, produced by cleavage of the BV-4 chromophore ring structure, have the wavelength position of its major absorption band moved toward the blue region, λ_{max}, **a**, 379.5 nm; **b**, 372.3 nm; **c**, 363.9 nm; **d**, 368.7 nm; **e**, 358.0 nm; **f**, 339.1 nm; **a′**, 379.5 nm, **b″**, 371.1 nm; **b′**, 374.7 nm; **c′**, 353.4 nm; and **d′**, 341.5 nm. The proposed intermediate (**a**) has been compared with standard material of 4-(*N*,*N*-diethylamino)-4′-(*N*′,*N*′-diethylamino)benzophenone. The retention time and absorption spectra are identical.

The fifth and sixth groups are marked in the chromatogram and illustrated in Figure 5b. The *N*-de-ethylation of the DAP, produced by cleavage of the BV-4 chromophore ring structure, has the wavelength position of its major absorption band moved toward the blue region, λ_{max}, α, 305.7 nm; β, 300.9 nm; and γ, 281.9 nm. The *N*-hydroxyethylated intermediate of the *N*-de-ethylated DAP species have the wavelength position of its major absorption band moved toward the blue region, λ_{max}, α′, 317.8 nm. The proposed intermediate (γ) has been compared with standard material of 4-aminobenzophenone. The retention time and absorption spectra are identical.

3.6.2. ESI-Mass Spectra of the Intermediates. The intermediates were further identified using the HPLC-ESI mass spectrometric method, and the relevant mass spectra are illustrated in Supporting Information (Figure 10). The molecular ion peaks appeared in the acid forms of the intermediates. The results of mass spectral analysis confirmed that the component **A**, m/z = 456.51, in liquid chromatogram is BV-4. The other components are **B**, m/z = 428.48; **C**, m/z = 400.46; **D**, m/z = 400.52; **E**, m/z = 372.44; **F**, m/z = 372.37; **G**, m/z = 344.41; **H**, m/z =

TABLE 1: Intermediates of the Photocatalytic Degradation of BV-4 Identified by HPLC-ESI-MS or GC-EI-MS with Conditions: 0.5 g L^{-1} TiO_2, 50 mg L^{-1} BV-4, Irradiation 20 h

HPLC peaks	intermediates[a]	abbreviation	MS peaks (*m/z*)	absorption maximum (nm)
A	*N*,*N*,*N*′,*N*′,*N*″,*N*″-hexaethylpararosaniline	BV-4	456.51	589.6
B	*N*,*N*-diethyl-*N*′,*N*′-diethyl-*N*″-ethylpararosaniline	DDEPR	428.48	584.7
C	*N*,*N*-diethyl-*N*′-ethyl-*N*″-ethylpararosaniline	DEEPR	400.46	577.3
D	*N*,*N*-diethyl-*N*′,*N*′-diethylpararosaniline	DDPR	400.52	578.9
E	*N*-ethyl-*N*′-ethyl-*N*″-ethyl pararosaniline	EEEPR	372.44	576.1
F	*N*,*N*-diethyl-*N*′-ethylpararosaniline	DEPR	372.37	578.6
G	*N*-ethy-*N*′-ethylpararosaniline	EEPR	344.41	567.6
H	*N*,*N*-diethylpararosaniline	DPR	344.41	573.7
I	*N*-ethylpararosaniline	EPR	316.39	556.6
J	pararosaniline	PR	288.30	550.3
A′	*N*,*N*-diethyl-*N*′,*N*′-diethyl-*N*″-hydroxyethyl-*N*″-ethylpararosaniline	DDHEPR	472.49	618.9
B′	*N*,*N*-diethyl-*N*′-hydroxyethyl-*N*′-ethyl-*N*″-ethylpararosaniline	DHEEPR	444.50	598.2
B″	*N*,*N*-diethyl-*N*′,*N*′-diethyl-*N*″-hydroxyethylpararosaniline	DDHPR	444.43	601.7
C′	*N*-hydroxyethyl-*N*-ethyl-*N*′-ethyl-*N*″-ethylpararosaniline	HEEEPR	416.47	578.6
C″	*N*,*N*-diethyl-*N*′-ethyl-*N*″-hydroxyethylpararosaniline	DEHPR	416.47	584.7
D′	*N*,*N*-diethyl-*N*′-hydroxyethyl-*N*′-ethylpararosaniline	DHEPR	416.41	585.9
E′	*N*-ethyl-*N*′-ethyl-*N*″-hydroxyethylpararosaniline	EEHPR	388.39	570.9
F′	*N*-hydroxyethyl-*N*-ethyl-*N*′-ethylpararosaniline	HEEPR	388.39	576.1
a	4-(*N*,*N*-diethylamino)-4′-(*N*′,*N*′-diethylamino)benzophenone	DDBP	325.41	379.5
b	4-(*N*,*N*-diethylamino)-4′-(*N*′-ethylamino)benzophenone	DEBP	297.38	372.3
c	4-(*N*-ethylamino)-4′-(*N*′-ethylamino)benzophenone	EEBP	269.29	363.9
d	4-(*N*,*N*-diethylamino)-4′-aminobenzophenone	DBP	269.29	368.7
e	4-(*N*-ethylamino)-4′-aminobenzophenone	EBP	241.33	358.0
f	4,4′-bis-aminobenzophenone	BP	213.17	339.1
a′	4-(*N*,*N*-diethylamino)-4′-(*N*′-hydroxyethyl-*N*′-ethylamino)benzophenone	DHEBP	341.36	379.5
b′	4-(*N*-hydroxyethyl-*N*-ethylamino)-4′-(*N*′-ethylamino)benzophenone	HEEBP	313.34	371.1
b″	4-(*N*,*N*-diethylamino)-4′-(*N*′-hydroxyethylamino)benzophenone	DHBP	313.40	374.7
c′	4-(*N*-ethylamino)-4′-(*N*′-hydroxyethylamino)benzophenone	EHBP	285.25	353.4
d′	4-(*N*-hydroxyethyl-*N*-ethylamino)-4′-aminobenzophenone	HEBP	285.31	341.5
α	4-(*N*,*N*-diethylamino)phenol	DAP	166.21	305.7
β	4-(*N*-ethylamino)phenol	EAP	N/A	300.9
γ	4-aminophenol	AP	N/A	281.9
α′	4-(*N*-hydroxyethyl-*N*-ethylamino)phenol	HEAP	N/A	317.8
I	*N*,*N*-diethylaminobenzene	DBz	149, 134,106, 77, 51	N/A
II	*N*-ethylaminobenzene	EBz	121, 106, 77	N/A
III	Aminobenzene	ABz	93, 66, 39	N/A
IV	Acetamide	AAm	59, 44, 43	N/A
V	2-Propenoic	PAc	72, 55, 45, 27	N/A
VI	Acetic	AAc	60, 45, 43	N/A

[a] Intermediates (**I**−**VI**) were identified by GC-MS, and the other intermediates were identified by HPLC-MS.

344.41; **I**, *m/z* = 316.39; **J**, *m/z* = 288.30; **A**′, *m/z* = 472.49; **B**′, *m/z* = 444.50; **B**″, *m/z* = 444.43; **C**′, *m/z* = 416.47; **C**″, *m/z* = 416.47; **D**′, *m/z* = 416.41; **E**′, *m/z* = 388.39; **F**′, *m/z* = 388.39; **a**, *m/z* = 325.41; **b**, *m/z* = 297.38; **c**, *m/z* = 269.29; **d**, *m/z* = 269.29; **e**, *m/z* = 241.33; **f**, *m/z* = 213.17; **a**′, *m/z* = 341.36; **b**′, *m/z* = 313.34; **b**″, *m/z* = 313.40; **c**′, *m/z* = 285.25; and **d**′, *m/z* = 285.31.

3.6.3. EI-Mass Spectra of the Partial Intermediates. The other intermediates were marked in the GC-MS/EI chromatogram (Figure 5c), and the relevant mass spectra are illustrated in Supporting Information (Figure 11). Table 1 presents the fragmentation patterns of the intermediates (**I**−**VI**) and the corresponding compounds identified by interpretation of their MS spectra. The peaks eluting at 30.48, 28.49, 25.61, 23.39, 17.57, and 12.38 min during GC-MS were identified as *N*,*N*-diethylaminobenzene, *N*-ethylaminobenzene, aminobenzene, acetamide, 2-propenoic acid, and acetic acid with fit values of 87%, 82%, 83%, 71%, 88%, and 95%, respectively, found by searching the mass spectra library (see Figure 11, Supporting Information). The intermediates identified in the study were also reported in a previous study of the methy lethyl ketone (MEK)/TiO_2 system.[28] Further oxidation of organic substrates containing nitrogen to nitrate can be obtained by increasing irradiation time. Results of HPLC chromatograms, UV−vis spectra, and HPLC-ESI and GC-EI mass spectra are summarized in Table 1.

3.6.4. Separation and Identification of Isomers. The absorption maximum of intermediates **D** (578.9 nm), **F** (578.6 nm), **H** (573.7 nm), and **d** (368.7 nm) occur at a longer wavelength than that of intermediate **C** (577.3 nm), **E** (576.1 nm), **H** (573.7 nm), and **c** (363.9 nm), respectively. These species correspond to the intermediates that possess from two to four (or two) ethyl groups relative to the BV-4 (or DDBP) dye and are correlative with three (or one) pairs of isomeric molecules. One of these isomers, DEEPR, is formed by removal of an ethyl group from two different sides of the BV-4 molecule while the other isomer in this pair, DDPR, is produced by removal of two ethyl groups from the same side of the BV-4 structure. In the second pair of isomers, EEEPR is formed by removal of an ethyl group from each side of the BV-4 molecule, and the other, DEPR, is formed by removal of both two-ethyl groups from the same side of the BV-4 structure and an ethyl group from the other side of the BV-4 structure. In the third pair of isomers, DPR is formed by removal of two ethyl groups from two different sides of the BV-4 molecule while EEPR is produced by removal of two ethyl groups from the same side of the BV-4 structure and of an ethyl group from the remaining two sides of the BV-4 structure. In the fourth pair of isomers, EEBP is formed by removal of an ethyl group from two different sides of the DDBP molecule while the other isomer in this pair, DBP, is produced by removal of two ethyl groups from the same side of the DDBP

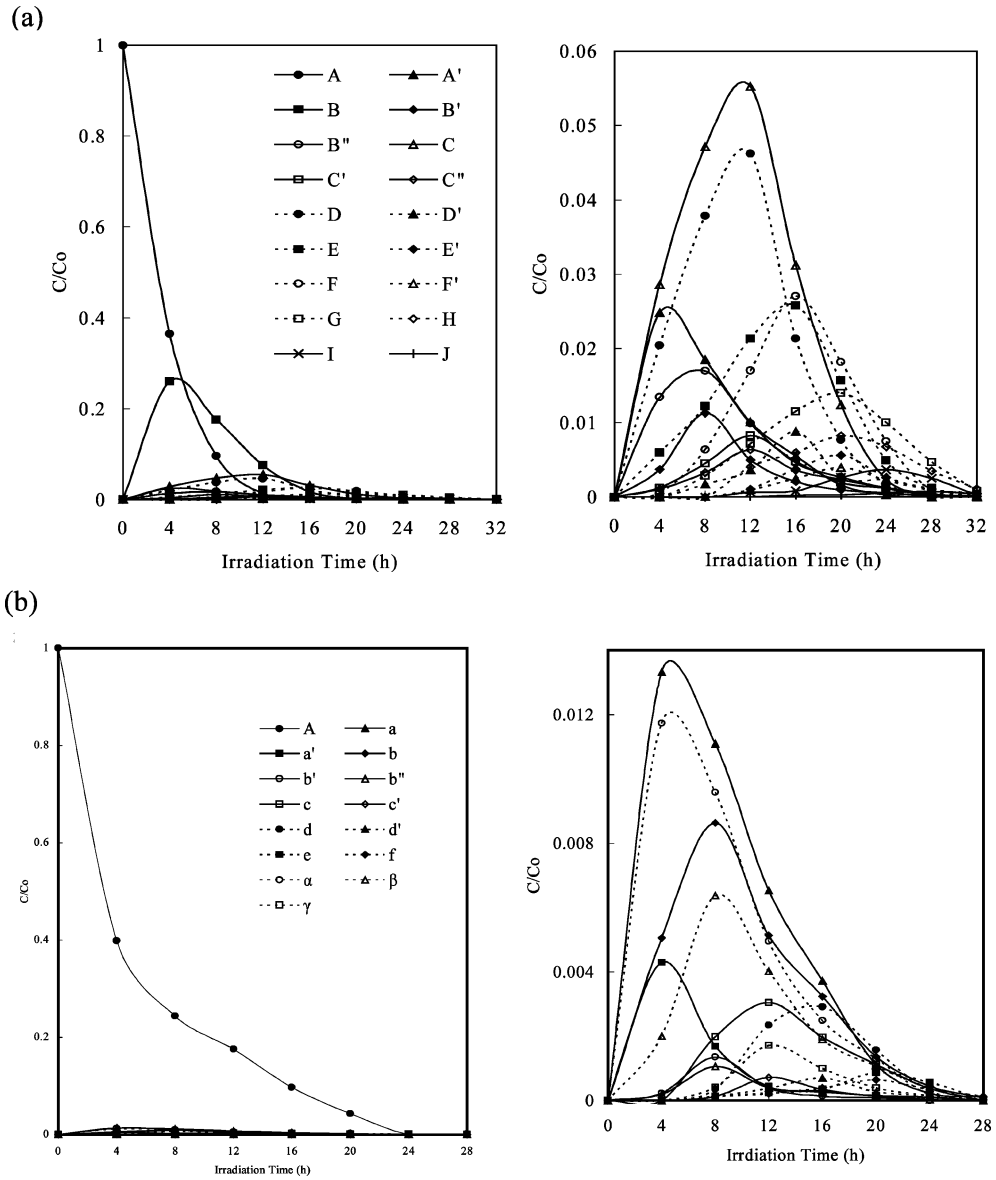

Figure 6. Variation in the relative distribution of the *N*-de-ethylated products obtained from the photodegradation of BV-4 as a function of irradiation time. Curves A−J and A′−F′ correspond to the peaks A−J and A′−F′ in Figure 5a, curves a−f, a′−d′, and α−γ correspond to the peaks a−f, a′−d′, and α−γ Figure 5b, respectively.

structure. Considering that the polarity of the DDPR, DEPR, DPR, and DBP species exceeds that of the DEEPR, EEEPR, EEPR, and EEBP intermediates, we expected the latter to be eluted after the former. Additionally, to the extent that two *N*-ethyl groups are stronger auxochromic moieties than are the *N*, *N*-diethyl or amino groups, the maximal absorption of the DDPR, DEPR, DPR, and DBP intermediates was anticipated to occur at wavelengths shorter than the band position of the DEEPR, EEEPR, EEPR, and EEBP species.

3.7. Photodegradation Mechanisms of BV-4. In an earlier study,[29] the formation of the *N*-methylamino moiety by the ozone attack on the *N*,*N*-dimethylamino group is explained by the initial electrophilic attack of ozone at the nitrogen atom. From the identical intermediate, the hydroxymethylamino derivatives are also obtained. Our identical intermediates, **A′**−**F′** (or **a′**−**d′**), are created by the *N*-de-ethylation of BV-4 (or DDBP) because the attack by one of the active oxygen species on the *N*,*N*-diethyl or *N*-ethyl group produced the hydroxyethylamino derivatives. As well, to the extent that the *N*-hydroxylethyl groups are weaker auxochromic moieties than are the *N*,*N*-diethyl or *N*-ethyl groups, the maximal absorption of the **A′**−**F′** intermediates was anticipated to occur at wavelengths longer than the band position of the **A**−**F** species, respectively. The following results and the proposed mechanism support this argument.

The relative distribution of the intermediates obtained is illustrated in Figure 6. To minimize errors, the relative intensities were recorded at the maximum absorption wavelength for each intermediate, although a quantitative determination of all of the photogenerated intermediates was not achieved, owing to the lack of appropriate molar extinction coefficients for them and owing to unavailable reference standards. The distributions of all of the *N*-de-ethylated intermediates are relative to the initial concentration of BV-4. Nonetheless, we clearly observed the changes in the distribution of each intermediate during the photodegradation of BV-4. The successive appearance of the maximum of each intermediate indicates that the *N*-de-ethylation of BV-4, DDBP, and DAP are a stepwise photochemical process by hydroxylated intermediates.

3.7.1. N-De-ethylation of BV-4. Most of the $^{\bullet}$OH radicals are generated directly from the reaction between the holes and the surface-adsorbed H_2O or OH^-. $O_2^{-\bullet}$ should be much less likely

SCHEME 1: Proposed *N*-de-ethylation Pathway of the BV-4 Dye under UV Irradiation in Aqueous TiO_2 Dispersions Followed by the Identification of Several Intermediates by HPLC-ESI Mass Spectral Techniques

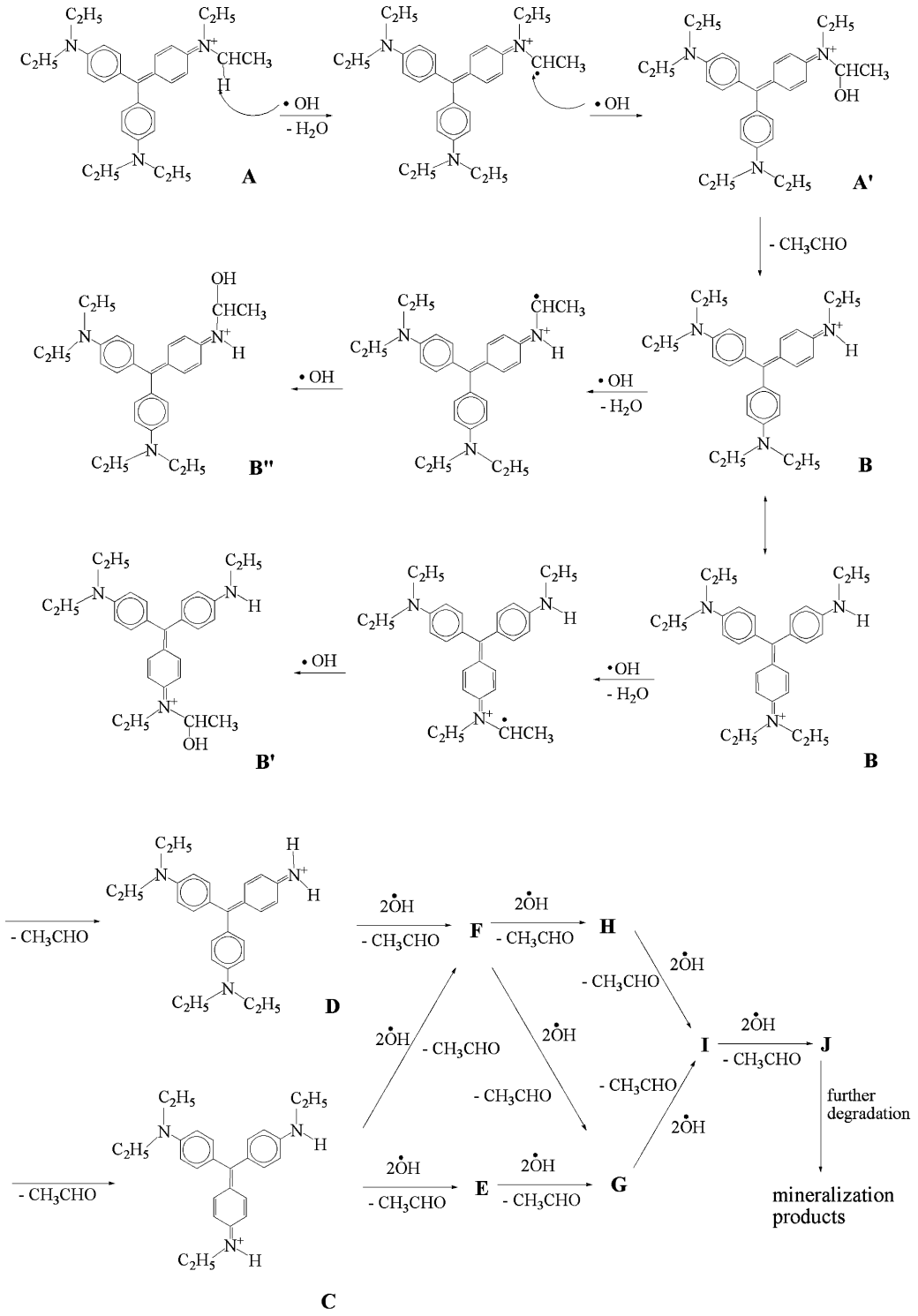

to be formed than •OH under UV irradiation.[18,19] The *N*-de-ethylation of the BV-4 dye occurs mostly through attack by the •OH species on the *N*,*N*-diethyl group of BV-4 under basic and neutral aqueous conditions. The *N*-mono-de-ethylated intermediate (DDEPR) was clearly observed (Figure 6a, curve B). The *N*-di-de-ethylated intermediates DEEPR and DDPR were clearly observed (curve C−D) to reach their maximum concentrations at the same time after a 12 h irradiation period. The *N*-tri-de-ethylated intermediate EEEPR was clearly observed (curve E−F) to reach its maximum concentration after a 16 h irradiation period while DEPR did so after 16 h because the •OH attacked the *N*-ethyl group of DEEPR and the *N*,*N*-diethyl group of DDPR. The *N*-tetra-de-ethylated intermediate EEPR was clearly observed (curve G−H) to reach its maximum concentration after a 20 h irradiation period because the •OH attacked the *N*-ethyl group of EEEPR and *N*,*N*-diethyl group of DEPR. DPR reached its maximum concentrations after a 20 h irradiation period because the •OH attacked the *N*,*N*-diethyl group of DEPR. DPR reached its maximum concentrations in the same irradiation time. In the *N*-penta-de-ethylated intermediate (EPR), (curve I), EPR reached its maximum concentration after a 24 h irradiation period because the •OH attacked the

SCHEME 2: Proposed Pathway of the Destruction of the Conjugated Structure of the BV-4 Dye under UV Irradiation in Aqueous TiO_2 Dispersions Followed by the Identification of Several Intermediates by HPLC-ESI Mass Spectral Techniques

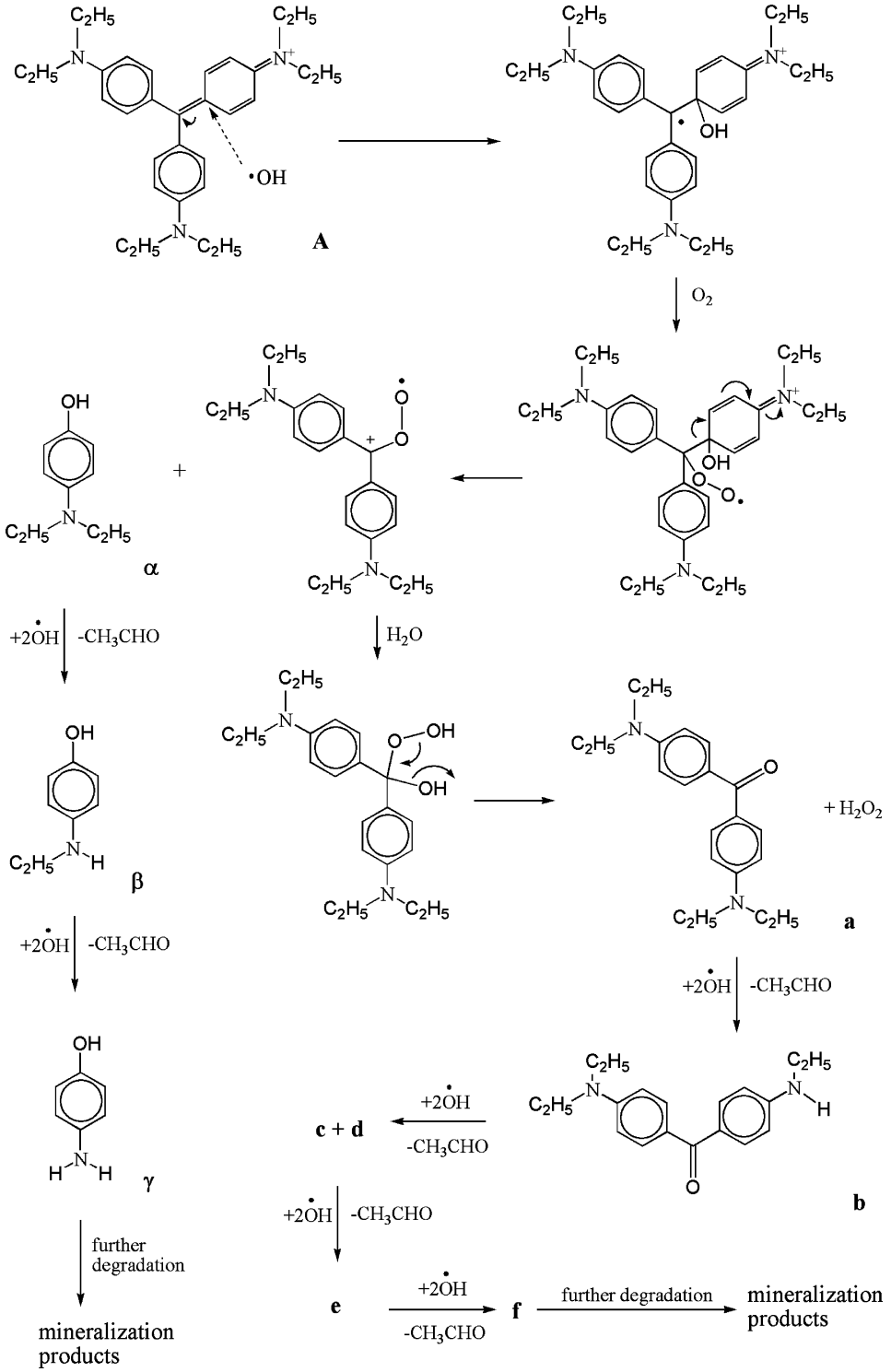

N-ethyl group of EEPR and attacked the *N*,*N*-diethyl group of DPR. In the *N*-hexa-de-ethylated intermediate (curve J), PR reached its maximum concentration after a 28 h irradiation period because the •OH attacked the *N*-ethyl group of EPR.

In the hydroxylation of *N*-hexa-ethylated intermediate, (curve **A′**), DDHEPR reached its maximum concentration after a 4 h irradiation period because of the •OH attack on the *N*,*N*-diethyl group of BV-4. In the hydroxylation of *N*-penta-ethylated intermediates, (curve **B′** and **B″**), DHEEPR and DDHPR reached their maximum concentrations after an 8 h irradiation period because of the •OH attack on the *N*,*N*-diethyl group of DDEPR and the *N*-ethyl group of DDEPR. In the hydroxylation of *N*-tetra-ethylated intermediates (curve **C′** and **C″**), HEEEPR and DEHPR reached their maximum concentrations after a 12 h irradiation period because the •OH attacked the *N*,*N*-diethyl group of HEEEPR and the *N*-ethyl group of DEHPR. In the hydroxylation of *N*-tetra-ethylated intermediates (curve **D′**), DHEPR reached its maximum concentration after a 16 h irradiation period because the •OH attacked the *N*,*N*-ethyl group of DDPR. In the hydroxylation of *N*-tri-ethylated intermediates

SCHEME 3: Proposed Pathway of the Destruction of the Conjugated Structure of the DDBP Derivatives (compounds I−VI) by the Identification of Six Intermediates by GC-EI Mass Spectral Techniques

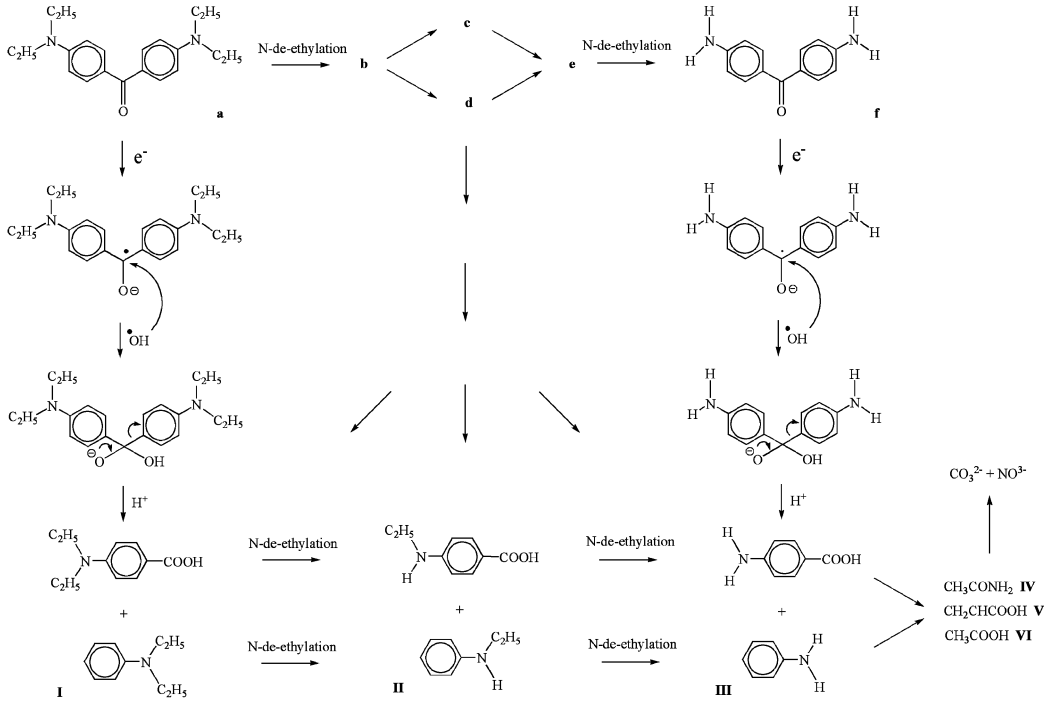

(curve **E′** and **F′**), EEHPR and DHPR reached their maximum concentrations after a 20 h irradiation period because the •OH attacked the *N*-ethyl group of EEEPR and the *N*,*N*-diethyl group of DEPR. The concentration of the other hydroxylated intermediates may be too low to be examined by HPLC-PDA-ESI-MS. The results discussed above can be seen more clearly from Scheme 1 and Table 1. BV-4 gets near the negatively charged TiO_2 particle surface via the positive diethylamine group. Then, before the destruction of the conjugated structure happened, the *N*-de-ethylation occurs preferentially with the major products being the *N*-de-ethylated BV-4 species and their *N*-hydroxyethylated intermediates.

3.7.2. Destruction of the Conjugated Structure of the BV-4. The degradation of the BV-4 dye occurs mostly through attack by the •OH species on the central carbon portion of BV-4 and produces DDBP and DAP under acidic aqueous conditions. The degradation intermediates DDBP and DAP were clearly observed (Figure 6b, curve a and α) to reach their maximum concentrations at the same time after a 4 h irradiation period. The *N*-mono-de-ethylated intermediates DEBP and EAP were clearly observed (curve b and *β*) to reach their maximum concentrations at the same time after an 8 h irradiation period. The *N*-di-de-ethylated intermediates (EEBP and AP) were clearly observed (curves c−d and *γ*) to have reached their maximum concentration after a 12 h irradiation period while DBP reached its maximum concentration after 16 h because the •OH attacked the *N*-ethyl group of DEBP and the *N*,*N*-diethyl group of DEBP. The *N*-tri-de-ethylated intermediate (EBP) was clearly observed (curve e) to have reached its maximum concentration after a 20 h irradiation period. In the *N*-tetra-de-ethylated intermediate (curve f), BP reached its maximum concentration after a 20 h irradiation period.

In the hydroxylation of DDBP (curve **a′**), DHEBP reached its maximum concentration after a 4 h irradiation period because the •OH attacked the *N*,*N*-diethyl group of DDBP. In the hydroxylation of DEBP (curve **b′** and **b″**), HEEBP and DHBP reached their maximum concentrations after an 8 h irradiation period because the •OH attacked the *N*,*N*-diethyl group of DEBP and the *N*-ethyl group of DEBP. In the hydroxylation of EEBP and DBP (curve **c′** and **d′**), HEEEPR and DEHPR reached their maximum concentrations after 12 and 16 h irradiation periods because the •OH attacked the *N*-ethyl group of EEBP and the *N*,*N*-diethyl group of DBP. The concentration of the other intermediates may be under the detection limit. The results we discussed above can be seen more clearly from Scheme 2 and Table 1. BV-4 is adsorbed on the positively charged TiO_2 particle surface via a conjugated structure. With the major photooxidation products being DDBP, DAP, their *N*-de-ethylated products, and via *N*-hydroxyethylated intermediates of the de-ethylated products, the cleavage of the BV-4 chromophore structure predominates, and *N*-de-ethylation occurs only to a slight extent.

Further evidence for the pathway(s) of photodegradation was obtained by GC-MS spectroscopic methods. From the results of mass spectral analysis, we identified the major component in the gas chromatograms as *N*,*N*-diethylaminobenzene, *N*-ethylaminobenzene, aminobenzene, acetamide, 2-propenoic acid, and acetic acid. The former intermediates (**I**−**III**) detected by GC-MS are the results of the cleavage of intermediates of the third group (**a**−**f**), leading to aminobenzene derivatives. The latter intermediates (IV−VI) were formed by cleavage of the aromatic derivatives, leading to aliphatic products. The results we discussed above can be seen more clearly from Scheme 3 and Table 1.

3.7.3. Pathways of Photocatalytic Degradation of the BV-4. According to earlier reports,[22,30−32] most *N*-de-alkylation processes are preceded by the formation of a nitrogen-centered radical while destruction of dye chromophore structures is preceded by the generation of a carbon-centered radical.[20,21,26,33,34] Consistent with this, degradation of BV-4 must occur via two different photodegradation pathways (destruction of the chromophore structure and *N*-de-ethylation) due to formation of different radicals (either a carbon-centered or nitrogen-centered radical). There is no doubt that the •OH attack on the dye yields a dye cationic radical. After this step, the cationic radical $Dye^{\bullet+}$ can undergo hydrolysis, follow various deprotonation pathways,

SCHEME 4: Proposed Pathway of Degradated BV-4 Dye under UV Irradiation in Aqueous TiO_2 Dispersion

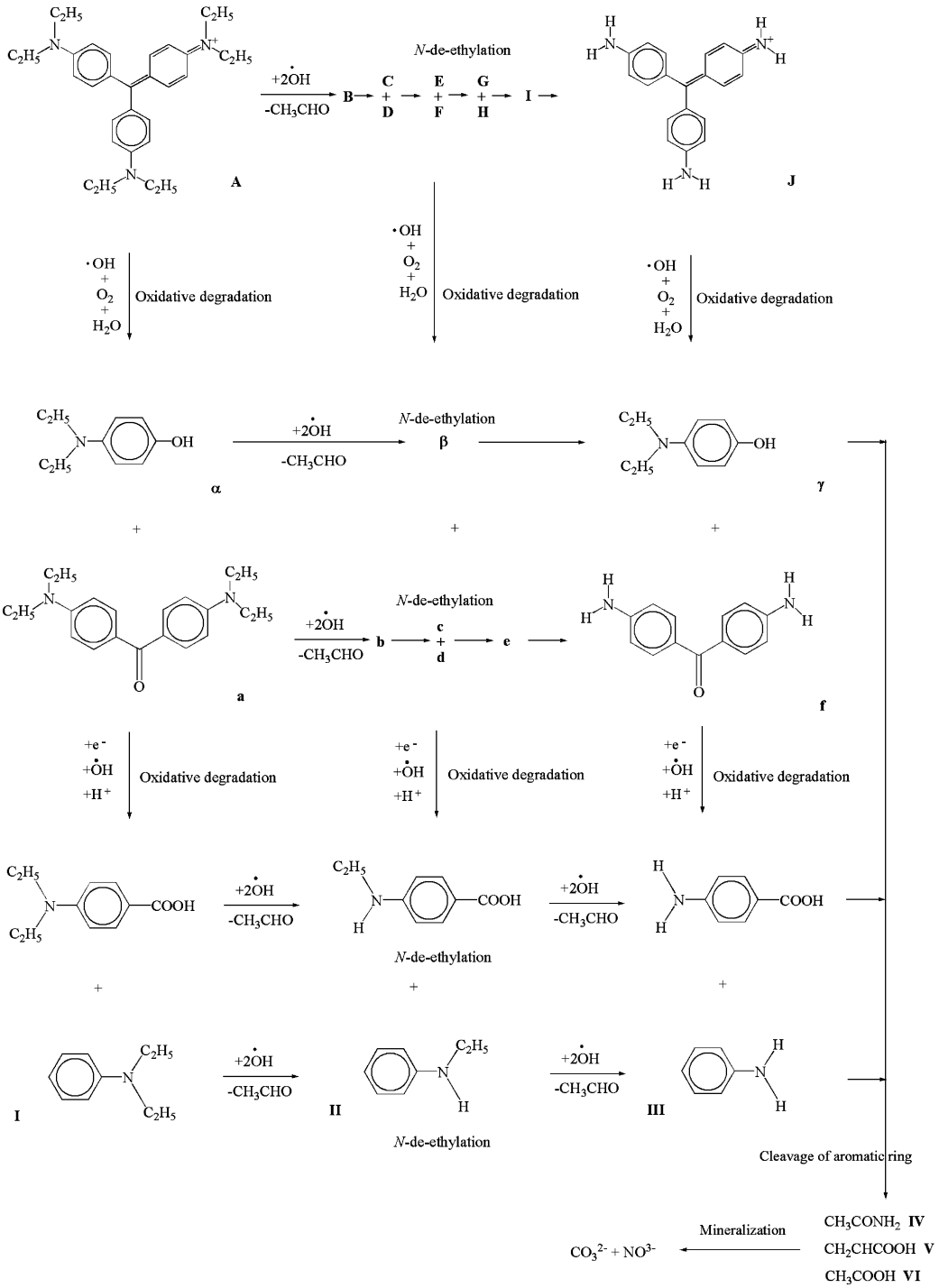

or both, which in turn are determined by the different adsorption modes of BV-4 on the TiO_2 particles surface.

On the basis of all of the above experimental results, we tentatively propose the pathway of photodegradation depicted in Scheme 4. In this scheme, the dye molecule in the BV-4/TiO_2 system is adsorbed through the positively charged diethylamine function. After one •OH radical attracted a hydrogen atom from ethyl group of diethylamine and another •OH radical attacked the diethylamine radical and formed hydroxyethylated intermediates, the subsequent hydrolysis (or deprotonation) of intermediates yields de-hydroxyethylated intermediates, which were subsequently attacked by •OH radicals to lead ultimately to *N*-de-ethylation. The mono-de-ethylated dye derivative, DDMPR, can also be adsorbed on the TiO_2 particle surface and be implicated in other similar events (•OH radicals attraction and attack, hydrolysis or deprotonation) to yield a bi-de-ethylated dye derivatives, DDPR and DMMPR. The *N*-de-ethylation process as described above continues until formation of the completely de-ethylated dye, PR.

In the Scheme 4, the dye molecule in the BV-4/TiO_2 system is adsorbed through a conjugated structure cleavage of the BV-4 chromophore structure. Following •OH radical attack the conjugated structure yields a carbon-centered radical, which is subsequently attacked by molecular oxygen to lead ultimately to DDBP and DAP. The same process happened in the *N*-de-ethylated dye to produce the *N*-de-ethylated DDBP and DAP. The DDBP can also be adsorbed on the TiO_2 particle surface and be implicated in other similar events (•OH radical attraction

and attack, hydrolysis or deprotonation, oxygen attack, or all three) to yield a mono-*N*-de-ethylated derivative, DEBP. Moreover, the same process happened in DAP to produce EAP. The *N*-de-ethylation process as described above continues until formation of the completely *N*-de-ethylated DDBP, BP, and *N*-de-ethylated DAP, AP. All of the above *N*-de-ethylation processes produced a series of *N*-de-hydroxyethylated intermediates by the hydroxylation on the *N*-ethyl group. All of the intermediates were further degraded to produce *N*,*N*-diethylaminobenzene, *N*-ethylaminobenzene, aminobenzene, acetamide, 2-propenoic acid, and acetic acid, which were subsequently mineralized to lead to CO_3^{2-} and NO_3^-.[24]

4. Conclusions

BV-4 could be successfully decolorized and degraded by TiO_2 under weak UV irradiation. The photodegradation efficiency of the BV-4 dye was found to increase with increasing value of pH. The photodegradation rate of the BV-4 dye was found to increase then decrease along with increases in the catalyst concentration. After 30 W UV 365 nm irradiation for 20 h, approximately 99.9% of the BV-4 was degraded.

Both *N*-de-ethylation and destruction of the conjugated structure of BV-4 take place in the presence of TiO_2 particles. The reaction mechanisms of TiO_2/UV proposed in this research would be useful for future application of the technology for decolorization of dyes.

Acknowledgment. This research was supported by the National Science Council of the Republic of China.

Supporting Information Available: HPLC chromatograms, UV−visible spectra, absorption spectra of photodecomposed intermediates, and ESI mass spectra of intermediates. This material is available free of charge via the Internet at http://pubs.acs.org.

References and Notes

(1) Peter, C. *Color in dye house effluent, the Society of Dyers and Colourists*; Alden Press: Oxford, U.K., 1995.
(2) Pagga, U.; Brown, D. *Chemosphere* **1986**, *15*, 479.
(3) Fox, M. A.; Duxbury, D. F. *Chem. Rev.* **1993**, *93*, 381.
(4) Ullmann's Encyclopedia of Industrial Chemistry, Part A27. *Triarylmethane and Diarylmethane Dyes*, 6th ed; Wiley-VCH: New York, 2001.
(5) Baptista, M. S.; Indig, G. L. *J. Phys. Chem. B* **1998**, *102*, 4678.
(6) Bonnett, R.; Martinez, G. *Tetrahedron* **2001**, *57*, 9513.
(7) Cho, B. P.; Yang, T.; Blankenship, L. R.; Moody, J. D.; Churchwell, M.; Bebland, F. A.; Culp, S. J. *Chem. Res. Toxicol.* **2003**, *16*, 285.
(8) Low, G. K. C.; McEvoy, S. R.; Matthews, R. W. *Environ. Sci. Technol.* **1991**, *25*, 460.
(9) Nohara, K.; Hidaka, H.; Pelizzetti, E.; Serpone, N. *J. Photochem. Photobiol. A: Chem.* **1997**, *102*, 265.
(10) Hoffman, M. R.; Martin, S. T.; Choi, W.; Bahnemann, W. *Chem. Rev.* **1995**, *95*, 69.
(11) Linsebigler, A. L.; Lu, G. Q.; Yate, J. T. *Chem. Rev.* **1995**, *95*, 735.
(12) Nasr, C.; Vinodgopal, K.; Fisher, L.; Hotchandani, S.; Chattopadhyay, A. K.; Kamat, P. V. *J. Phys. Chem.* **1996**, *100*, 8436.
(13) Chen, C. C.; Li, X.; Zhau, J. C.; Hidaka, H.; Serpone, N. *J. Phys. Chem. B* **2002**, *106*, 318.
(14) Chu, W.; Wong, C. C. *Environ. Sci. Technol.* **2003**, *37*, 2310.
(15) Lee, J.; Choi, W.; Yoon, J. *Environ. Sci. Technol.* **2005**, *39*, 6800.
(16) Chen, C. C.; Lu, C. S. *Environ. Sci. Technol.* **2007**, *41*, 4389.
(17) Nakamura, R.; Nakato, Y. *J. Am. Chem. Soc.* **2004**, *126*, 1290.
(18) Murakami, Y.; Kenji, E.; Nosaka, A. Y.; Nosaka, Y. *J. Phys. Chem. B* **2006**, *110*, 16808.
(19) Wu, T.; Liu, G.; Zhao, J. C.; Hidaka, H.; Serpone, N. *J. Phys. Chem. B* **1998**, *102*, 5845.
(20) Li, X.; Liu, G.; Zhao, J. C. *New J. Chem.* **1999**, *23*, 1193.
(21) Liu, G.; Li, X.; Zhao, J. C.; Hidaka, H.; Serpone, N. *Environ. Sci. Technol.* **2000**, *34*, 3982.
(22) Chen, C. C.; Lu, C. S.; Chung, Y. C. *J. Photochem. Photobiol. A: Chem.* **2006**, *181*, 120.
(23) Parra, S.; Stanca, S. E.; Guasaquillo, I.; Thampi, K. R. *Appl. Catal., B* **2004**, *51*, 107.
(24) Prevot, A. B.; Baiocchi, C.; Brussino, M. C.; Pramauro, E.; Savarino, P.; Augugliaro, V.; Marci, G.; Palmisano, L. *Environ. Sci. Technol.* **2001**, *35*, 971.
(25) Zhao, J. C.; Hidaka, H.; Takamura, A.; Pelizzetti, E.; Serpone, N. *Langmuir* **1993**, *9*, 1646.
(26) Liu, G.; Wu, T.; Zhao, J.; Hidaka, H.; Serpone, N. *Environ. Sci. Technol.* **1999**, *33*, 2081.
(27) Kerr, G. H.; Meth-Cohn, O. *J. Chem. Soc. C* **1971**, 1369.
(28) Lu, C. S.; Chen, C. C.; Mai, F. D.; Wu, Y. C. *J. Photochem. Photobiol., A* **2007**, *187*, 167.
(29) Galliani, G.; Rindone, B.; Scolastico, C. *Tetrahedron Lett.***1975**, 1285.
(30) Shaefer, F. C.; Zimmermann, W. D. *J. Org. Chem.* **1970**, *35*, 2165.
(31) Laube, B. L.; Asirvatham, M. R.; Mann, C. K. *J. Org. Chem.* **1977**, *42*, 670.
(32) Zhao, J. C.; Wu, T.; Wu, K.; Oikawa, K.; Hidaka, H.; Serpone, N. *Environ. Sci. Technol.* **1998**, *32*, 2394.
(33) Wu, T.; Lin, T.; Zhao, J. C.; Hidaka, H.; Serpone, N. *Environ. Sci. Technol.* **1999**, *33*, 1379.
(34) Liu, G.; Zhao, J. C. *New J. Chem.* **2000**, *24*, 411.